JOURNAL OF Materials CHEMISTRY

# Fast, reversible optical sensing of $NO_2$ using 5,10,15,20-tetrakis[3,4-bis(2-ethylhexyloxy)phenyl]-21*H*,23*H*-porphine assemblies†

**Colin M. Dooling,[a] Oliver Worsfold,[a] Tim H. Richardson,*[a] Rose Tregonning,[b] M. O. Vysotsky,[b] Chris A. Hunter,[b] Keizo Kato,[c] Kazunari Shinbo[c] and Futao Kaneko[c]**

[a]*Applied Molecular Engineering Group, Department of Physics & Astronomy, University of Sheffield, Hounsfield Road, Sheffield, UK S3 7RH. E-mail: t.richardson@sheffield.ac.uk*
[b]*Department of Chemistry, University of Sheffield, Dainton Building, Brook Hill, Sheffield, UK S3 7HF*
[c]*Graduate School of Science and Technology, Niigata University, Niigata, Japan*

***Received 3rd August 2000, Accepted 2nd November 2000***
***First published as an Advance Article on the web 14th December 2000***

The optical absorbance spectrum of LB film assemblies of 5,10,15,20-tetrakis[3,4-bis(2-ethylhexyloxy)phenyl]-21*H*,23*H*-porphine (EHO) is highly sensitive to low concentrations of $NO_2$ in nitrogen. LB films prepared at much faster than conventional deposition rates ($\sim$1000 mm min$^{-1}$) yield $t_{50}$ response and recovery times of 25 s and 33 s respectively and show a sensitivity of 60% relative absorbance change (at 430 nm) for 4.4 ppm $NO_2$. The morphology of these films is revealed using atomic force microscopy to contain isolated micron-size domains which are themselves composed of grains of several nm in diameter. This unconventional structure leads to a useful sensing material as a result of the molecular functionality of the porphyrin coupled to the enhanced surface area of the porous film assembly. The EHO film shows a gradually diminishing optical response as its temperature is increased, resulting from the shift in the adsorption–desorption equilibrium towards desorption as expected. The UV–visible spectrum recovers fully after exposure to $NO_2$. The rate of recovery is slow at room temperature but can be accelerated dramatically with gentle heating ($\sim$350 K) for a few seconds. The concentration dependence of the optical response over the range 0.8–4.4 ppm follows a Langmuir model.

## Introduction

The ability to detect toxic gases such as $NO_2$, $Cl_2$, HCl, $SO_2$, $H_2S$, CO and $NH_3$ in a wide range of environments has become progressively important over the last decade as a result of increased toxic gas production in the chemical industry.[1] In parallel with this has arrived ever more stringent health, safety and environmental legislation which should ensure that toxic substances have a reduced effect on human and environmental well-being.[2] However, this will only be confirmed provided that more sensitive gas sensors continue to be developed for monitoring at lower concentration levels. This, coupled to the economic requirements to produce ever less expensive sensors, provides the motivation for further gas sensor research.

The most commonly used toxic gas sensors are those based on semiconducting metal oxides[3] such as tin oxide, the niobates, the perovskites and the tungsten oxides. These devices operate as a result of a gas-sensitive electrical conductivity and normally require relatively high operating temperatures (400–600 °C). Other well-known sensor types include liquid electrolyte fuel cells and infra-red sensors.[3]

Some attention has been directed towards organic materials as candidates for gas sensors. Most notably, certain conducting polymers[4] arguably have achieved limited success in "electronic nose" applications, and phthalocyanines have attracted a great deal of interest as organic semi-conductometric sensors.[5] On most occasions, however, the least attractive features of the majority of such organic sensors have been their relatively slow gas response time (typically in the range 5–10 minutes for $t_{50}$, the time taken for the measured sensor property to evolve to 50% of its final value) and their incomplete recovery after gas exposure.

Porphyrins[6] and their derivatives have also been investigated although not as thoroughly as phthalocyanines. Recently a class of sulfonamidotetraphenylporphyrins have shown promise as useful sensing materials for chlorine in particular.[7] Porphyrins are generally less conducting than most phthalocyanines but share the common property of possessing rich UV–visible absorption spectra owing to their highly conjugated π-electron systems.[8] The extended range of wavelengths now available as narrow-band light sources in the form of either light emitting diodes or laser diodes suggests that porphyrin assemblies merit further study as potentially useful sensing materials.

In this paper, the $NO_2$ sensitivity of 5,10,15,20-tetrakis[3,4-bis(2-ethylhexyloxy)phenyl]-21*H*,23*H*-porphine (EHO, Fig. 1) has been studied in the solution and solid state.

## Experimental

### Synthesis of EHO

**Materials.** UV–Visible electronic absorption spectra (solution) were recorded on a Cary 3 Bio UV–Visible spectrophotometer using quartz cuvettes. Fast atom bombardment (+ve FAB) mass spectra were obtained on a Fisons/VG Pro Spec 3000 using a *m*-nitrobenzyl alcohol matrix. Column chromatography was carried out using Florisil 100–200 mesh (Aldrich) and silica gel (40–63 μm). Nuclear magnetic resonance (NMR) spectroscopy was performed on a Bruker AM-

†Notes on ultra-fast LB deposition are available as supplementary data. For direct elctronic access see http://www.rsc.org/suppdata/jm/b0/b006342h/

 DOI: 10.1039/b006342h

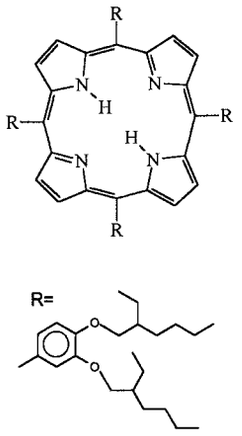


**Fig. 1** Chemical structure of EHO.

250 MHz or a AMX-400 MHz spectrometer as indicated. All operated as Fourier transform machines. All spectra were referenced to $CHCl_3$. Melting points were performed on a Reichter Kofler hot stage melting point apparatus.

Dichloromethane was supplied by Fisher and was stabilised with amylene (0.02%). It was purified and dried by distillation over calcium hydride. Dry ethanol was obtained by distillation over molecular sieves (4 Å) and stored over molecular sieves (4 Å). Triethylamine was dried by storage over 4 Å molecular sieves.

3,4 Dihydroxybenzaldehyde and 2-ethylhexyl bromide were supplied by Lancaster. Aldrich supplied all other reagents. All reagents were used as received except pyrrole, which was distilled fresh on the day of use.

## Synthesis

The synthesis and structure of 5,10,15,20-tetrakis[3,4-bis(2-ethylhexyloxy)phenyl]-21*H*,23*H*-porphine (EHO) is outlined below.

**3,4-Bis(2-ethylhexyloxy)benzaldehyde.** 2-Ethylhexyl bromide (5.60 mL, 0.031 mol) was added dropwise to a stirred solution of 3,4-dihydroxybenzaldehyde (2.07 g, 0.015 mol) and potassium carbonate (6.20 g, 0.045 mol) in butanone (60 mL) under conditions of reflux. These conditions were maintained for a period of four days after which the reaction mixture was filtered through Celite and the solvent was removed under vacuum to yield a dark brown oil. This was then re-dissolved in ether (50 mL), washed with 1 M NaOH ($1 \times 50$ mL), $H_2O$ ($1 \times 50$ mL) and brine ($1 \times 50$ mL) and then dried over $Na_2SO_4$. The solution was again filtered and the solvent was removed under vacuum before purification by column chromatography [silica, eluant petroleum ether (bp 40–60 °C)–ethyl acetate, 9 : 1] to give the product as a mixture of diastereoisomers in the form of a pale yellow oil (4.49 g, 83%).

$^1$H NMR 250 MHz ($CDCl_3$): $\delta$ (ppm) = 9.81 (s, 1H), 7.39 (dd, 1H, $^3J_{HH}$ = 7.9 Hz, $^4J_{HH}$ = 1.8 Hz), 7.37 (s, 1H), 6.92 (d, 1H, $^3J_{HH}$ = 7.9 Hz), 3.91 (t, 4H, $^3J_{HH}$ = 6.1 Hz), 1.76 (septet, 2H, $^3J_{HH}$ = 4.3 Hz), 1.2–1.6 (m, 16H), 0.8–1.0 (m, 12H). $^{13}$C NMR 250 MHz ($CDCl_3$): $\delta$ (ppm) = 200.8, 190.9, 155.0, 151.9, 149.8, 149.6, 142.5, 130.8, 129.8, 127.2, 126.6, 123.8, 122.9, 112.7, 111.8, 111.4, 110.4, 71.5, 71.3, 60.3, 39.6, 39.5, 39.4, 39.2, 33.6, 30.9, 30.6, 30.5, 29.1, 28.8, 23.9, 23.8, 23.7, 23.0, 22.8, 22.6, 20.9, 19.4, 14.0, 13.9, 11.2, 11.0, 8.3. HR-FAB-MS, *m*/*z*: 363.2890 ($M^+$) (Calc. for $C_{23}H_{38}O_3$ 363.2899).

**5,10,15,20-Tetrakis[3,4-bis(2-ethylhexyloxy)phenyl]-21*H*,23*H*-porphine.** In the absence of light 3,4-bis(2-ethylhexyloxy)benzaldehyde (1813 mg, 5 mmol) was dissolved in a mixture of dry dichloromethane (500 mL), dry ethanol (3.25 mL) and freshly distilled pyrrole (347 μL, 5 mmol). This was then stirred under nitrogen for 10 minutes before the addition of boron trifluoride–diethyl ether (0.25 mL, 2 mmol), after which stirring was continued under nitrogen atmosphere and in the absence of light for a further 90 minutes. 2,3-Dichloro-5,6-dicyano-1,4-benzoquinone (1.138 mg, 5 mmol) was then added to the mixture and the conditions maintained for a further 90 minutes before the addition of triethylamine (2.80 mL, 20 mmol). Solvent was then removed under vacuum and the resulting solid was extracted with methanol ($32 \times 100$ mL) using a soxhlet apparatus. The residue was then purified by column chromatography [Florisil, eluant chloroform–petroleum ether (bp 40–60 °C), 38 : 62]. The porphyrin fractions were further purified by column chromatography [silica, eluant chloroform–petroleum ether (bp 40–60 °C), 38 : 62]. The product was then recrystallised from chloroform–methanol to yield a purple solid (655 mg, 32%).

$^1$H NMR 250 MHz ($CDCl_3$): $\delta$ (ppm) = 8.91 (s, 8H), 7.76 (d, 4H, $^4J_{HH}$ = 2.0 Hz), 7.69 (d, 4H, $^3J_{HH}$ = 8.2 Hz), 7.23 (d, 4H, $^3J_{HH}$ = 8.2 Hz), 4.17 (d, 8H, $^3J_{HH}$ = 5.8 Hz), 3.97 (d, 8H, $^3J_{HH}$ = 5.8 Hz), 1.95 (septet, 4H, $^3J_{HH}$ = 6.0 Hz), 1.81 (septet, 4H, $^3J_{HH}$ = 6.0 Hz), 1.12–1.80 (m, 64H), 0.8–1.10 (m, 48H), −2.8 (s, 2H). $^{13}$C NMR 250 MHz ($CDCl_3$): $\delta$ (ppm) = 149.4, 147.5, 134.9, 127.6, 120.7, 120.1, 111.6, 71.9, 41.0, 39.9, 39.2, 31.9, 30.8, 29.8, 29.3, 25.2, 24.1, 23.2, 14.2, 11.4. FAB-MS (+ve), *m*/*z*: 1642 (100%, $MH^+$) (Calc. for $C_{108}H_{158}N_4O_8$ 1640.46). UV–VIS ($CHCl_3$): $\lambda_{max}$/nm ($\varepsilon \times 10^{-3}$ mol$^{-1}$ l cm$^{-1}$) = 427 (368), 522 (18), 556 (13), 592 (7), 651 (7). Melting point: 146 °C.

## Langmuir isotherm measurement

The Langmuir isotherm for EHO was measured using a NIMA 1060 Langmuir trough. EHO was spread from a chloroform solution (50 μl) of concentration 0.129 mg ml$^{-1}$ onto a water subphase using a Hamilton microsyringe (pH ~ 6.2, 296 K). After evaporation of the solvent, the floating Langmuir film was compressed at a rate of 15 cm$^2$ min$^{-1}$ (~30% min$^{-1}$).

## Ultra-fast deposition technique

Conventionally, the Langmuir–Blodgett deposition process is considered to be a relatively slow coating process and indeed, this is one of the reasons it has remained commercially unattractive. Although there have been attempts to deposit conventional fatty acid materials at high transfer rates,[9] very seldom have linear deposition rates greater than 50 mm min$^{-1}$ been adopted for more exotic LB film-forming materials. In this work, very high deposition rates of 1000 mm min$^{-1}$ were used for the porphyrin under study. Hydrophobically treated glass substrates (BDH Super Premium microscope slides treated with 1,1,1,3,3,3-hexamethyldisilazane) were used, and the gain control of the constant-perimeter Langmuir trough (Joyce–Loebl mini-trough) was set at its maximum value to allow the compression barrier to respond as quickly as possible to the slight surface pressure decrease that occurred during transfer. This is particularly important when the transfer rate is high.

## Atomic force microscopy

The atomic force microscopy (AFM) was carried out at room temperature in air by tapping mode using a Nanoscope IIIa (Digital Instruments) microscope.

## Gas testing

The thin film samples were sliced into small segments approximately 1 cm × 2.5 cm and placed in a purpose-built gas testing chamber (Fig. 2). This consisted of a gas inlet and an outlet, a Peltier heating–cooling stage and housings for fibre optic cables supplying the probe light beam from the tungsten

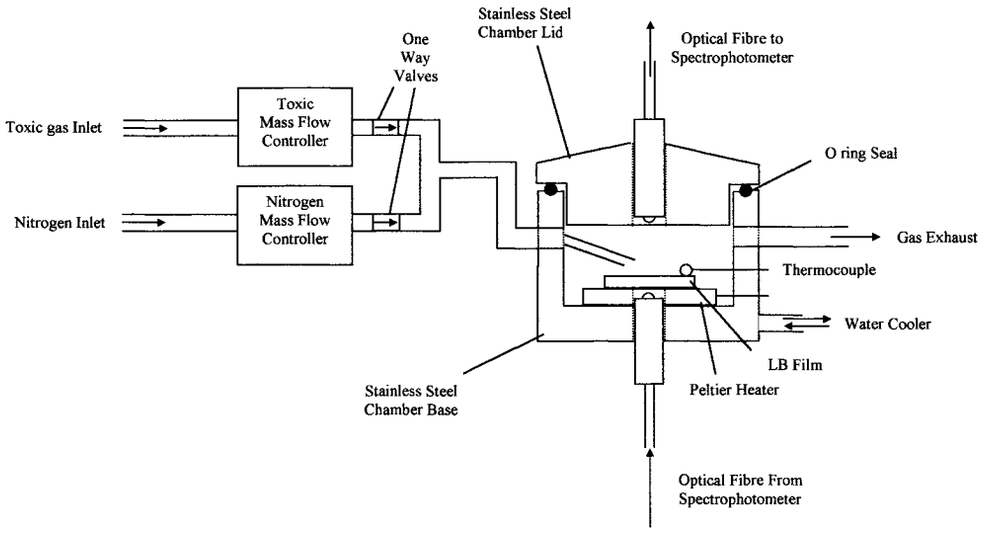


**Fig. 2** Schematic diagram of gas testing apparatus.

white light source and delivering the light transmitted through the sample to the optical detector. Two gas cylinders were used, one containing 4.4 ppm (parts per million) $NO_2$ (precisely mixed by BOC, UK) and the other containing dry nitrogen. The flow rates of these gases were moderated by two computer-controlled Tylan FC-260 mass flow controllers in order that the gas concentration after subsequent mixing could be precisely selected in the range 0.1–4.4 ppm. In normal operation, the exposure of the sample to the $NO_2$ occurred at room temperature ($\sim$293 K) and the recovery phase (dry nitrogen only) occurred at elevated temperature (353 K). These conditions were used in all experiments unless otherwise stated.

Optical measurements were performed using a World Precision Instruments "Spectromate" spectrophotometer. This instrument utilises a multi-channel photodiode array and can therefore enable spectra across the entire visible region to be collected in a short period of time. In this study, data were collected typically every 2–4 s during exposure of the sample to the toxic gas stream and to the dry nitrogen gas during the recovery cycle. In addition to the spectra being recorded every few seconds, the instrument would also display changes in the optical absorbance (at selected wavelengths) as a function of time, thus allowing the kinetics of the adsorption and desorption processes to be followed.

## Results and discussion

### Surface pressure–area isotherm

Fig. 3 shows the surface pressure–area isotherm of EHO. A quasi-solid region of the isotherm is observed over the surface pressure range 8–18 mN m$^{-1}$ before a slight kink appears prior to the onset of another incompressible phase occurring above

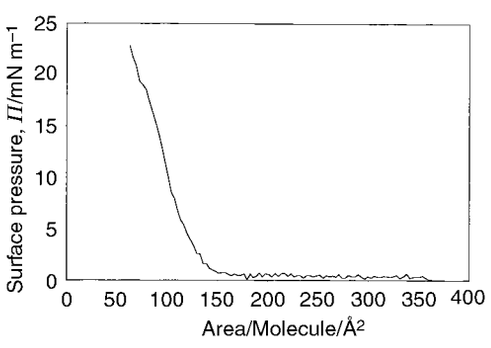


**Fig. 3** Surface pressure–area isotherm for EHO.

19 mN m$^{-1}$. Extrapolation of the former quasi-solid region of the isotherm to zero surface pressure yields an area per molecule of $\sim$125 Å$^2$. This value most probably represents an orientation in which the porphyrin ring faces down onto the water surface with the substituted alkyl groups protruding from the plane of the water surface. Modelling (using CPK space-filled models) of such an orientation would yield an area per molecule of $\sim$150 Å$^2$; the difference in the two values occurs most probably as a result of either a degree of aggregation within the monolayer (*i.e.* non-monolayer aggregate regions within a monolayer host) or a tilted porphyrin orientation in which the plane of the porphyrin core is tilted with respect to the plane of the water surface. Normally, thickness studies could be used to verify the orientation of the molecules within a Langmuir film. Here, however, as a result of the ultra-fast deposition technique employed, the resulting inhomogeneous, perforated film structure does not provide a well-defined film thickness to be used in conjunction with isotherm measurements. In common with conventional LB films deposited more slowly (typically 0.1–10 mm min$^{-1}$), LB films produced *via* ultra-fast deposition do grow in a layer-by-layer fashion as evidenced by the gradual linear build up in optical absorbance as a function of number of passages of the substrate through the floating Langmuir film (ESI). The average optical absorbance per monolayer is $\sim$0.025 which is consistent with monolayer values obtained previously for porphyrins and phthalocyanines by other authors.[7,8] In this measurement, a relatively large light beam width ($\sim$2 mm) has been used in order to average over many EHO domains.

### Atomic force microscopy

Fig. 4 is an atomic force microscope image of a 20 monolayer EHO film deposited at 1000 mm min$^{-1}$ onto an optically flat glass substrate. The image shows a disordered array of "islands" of EHO distributed over the surface. The underlying substrate can be observed between some of these islands (and indeed has been imaged separately in addition) and indicates that the topology of the EHO assembly does not arise simply as a result of the substrate surface roughness. It is thought that the mechanism for the formation of these islands arises from dewetting of the substrate film during transfer from the water surface.

Traditionally, researchers have defined useful LB films to be highly uniform, ordered and relatively dense molecular assemblies. However, for certain applications these features are actually detrimental to performance. One such application is the main topic of this paper, namely gas sensing. In this case,

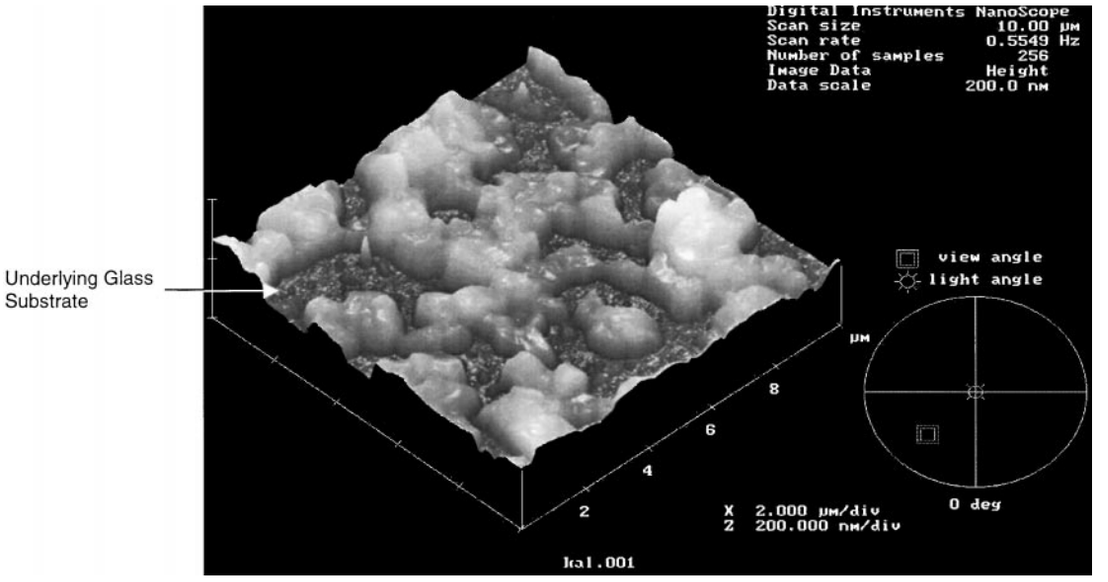


**Fig. 4** Atomic force microscope image of a 10 excursion LB film of EHO deposited at 1000 mm $min^{-1}$.

a relatively porous macrostructure is required in order to promote ingress and egress of the analyte gas into and from the thin film. This also enhances the surface area of the sensing film. Thin film gas sensing is primarily characterised by a fast surface adsorption process (often followed by a much slower diffusion into the bulk) and therefore modifications to the macrostructure that augment the surface area are advantageous.

Analysis of this image has shown that the height of the EHO domains within the LB assembly is significantly larger than the expected height for 20 monolayers. One might have expected a thickness per transferred layer of around 1.3 nm, but a height profile study of the image shown reveals that the typical domain height is around $\sim$55 nm. The transfer ratio (corresponding to the ratio of the area of the floating monolayer to the area of the substrate drawn through the air–water interface) is close to unity. Although a qualitative approach, the average domain height is $\sim$2.7 nm per transferred monolayer (55 nm per 20 "layers") and observation of the image suggests that the surface coverage is approximately 50%. This supports the idea that material absent from certain uncovered areas of the substrate has been "drawn into" the domains of EHO during or just after deposition. The EHO domains are typically around $0.8 \times 0.8$ µm in dimension although the distribution of domain size is wide; some of these coalesce together to form larger features. The surface roughness of each domain is typically $\sim$4–12 Å and that of the substrate is around 3–4 Å. Each domain is composed of small "grains" of characteristic lateral dimension $\sim$30 nm. The growth of these grains and the formation of the EHO domains is a major topic of further investigation.

### UV–visible spectroscopy: gas-sensitive optical properties

The UV–visible absorbance spectra of a solution of EHO (with a chloroform solvent) through which an $NO_2$ gas stream ($\sim$4 ppm) was bubbled are shown in Fig. 5. Before any exposure to $NO_2$, the characteristic porphyrin spectrum is observed with an intense Soret band appearing at $\sim$425 nm along with weaker Q-bands in the region 500–700 nm. As the bubbling proceeds, a dramatic change in the spectrum develops, involving the weakening of the Soret band intensity and the simultaneous growth of a band around 465 nm which is coupled to a further band at 700 nm. Such spectral changes could indicate protonation of the porphyrin or oxidation. The absorbance spectrum reverses (not shown) to its original form several hours after switching off the gas stream. It should be noted that there are no bathochromic or hypsochromic shifts in the wavelengths of any of the three main spectral bands present (425 nm, 465 nm and 700 nm) during the exposure. This is not surprising since such shifts are normally indicative of a change in the aggregation state of the solute molecules. In the dilute solution ($\ll$0.1 mg $ml^{-1}$) however, little or no aggregation exists and therefore no such shifts are expected.

Fig. 6 shows the temporal evolution of the absorbance spectrum of a nominally 6 monolayer transferred film (note

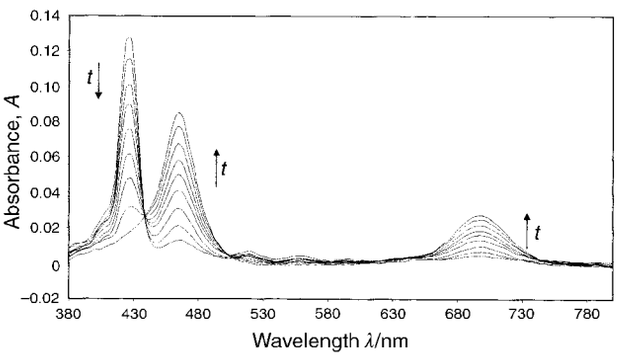


**Fig. 5** The time evolution of the UV–visible spectrum of a chloroform solution of EHO during exposure to 4.4 ppm $NO_2$ gas (time interval is 10 s).

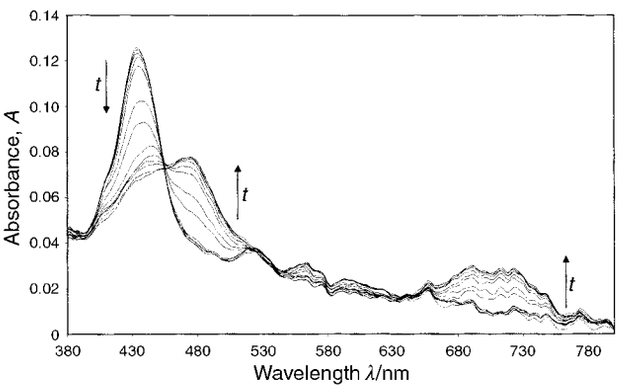


**Fig. 6** The time evolution of the UV–visible spectrum of an LB film (3 excursions) of EHO during exposure to 4.4 ppm $NO_2$ gas (time interval is 4 s).

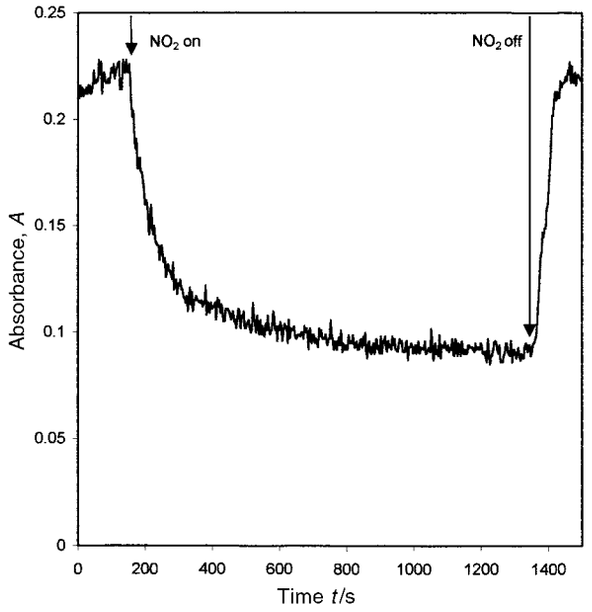


**Fig. 7** Absorbance of the Soret band (430 nm) of an LB film of EHO (6 excursions) as a function of time during exposure to 4.4 ppm $NO_2$.

that this refers to a sample which has made 3 transits through the floating monolayer in both directions). The initial pre-exposure spectrum (highest intensity of the Soret band) is significantly broader than that of the solution (Fig. 5); its FWHM is ~45 nm compared with ~17 nm for the solution. This is attributed to the crystal field effect for the relatively closely packed porphyrin molecules in the thin film assembly. The peak wavelength of the Soret band for the solid film is bathochromically shifted by ~7 nm with respect to the solution, and this shift further develops during the gas exposure. Similarly, the lower wavelength band forming as a result of the gas exposure develops at 480 nm compared to 465 nm for the solution. These bathochromic shifts are again attributed to the aggregation state of the porphyrin in the thin film.[10] The band at 700 nm also evolves in the solid state, although it is relatively weak and very broad. It should be noted that no sensitivity to $NO_2$ gas was observed for a solution cast film prepared by simply allowing droplets of the chloroform solution to fall onto the substrate.

The kinetics of the gas exposure (293 K) and recovery

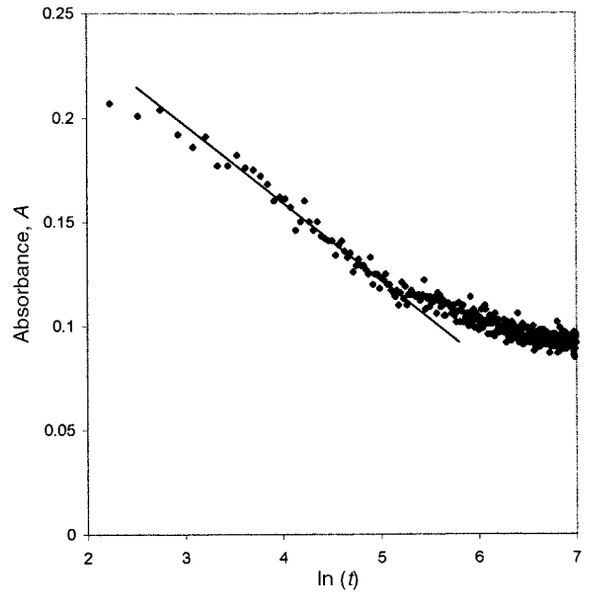


**Fig. 8** Elovich plot for an EHO LB film.

**Table 1** The $t_{50}$ and $t_{90}$ values for response and recovery phases for an EHO LB film

| | $t_{50}$/s | $t_{90}$/s |
|---|---|---|
| Response phase | 25 | 190 |
| Recovery phase | 33 | 73 |

(353 K) can be seen from Fig. 7 which shows the absorbance of the Soret band (430 nm) as a function of time. The decay of the Soret band intensity during the gas exposure has been found to fit an Elovichian kinetics model[11] most readily. This model states that the rate of coverage, $q$, of the film surface ($dq/dt$) is given by eqn. (1):

$$dq/dt = ae^{-bq} \quad (1)$$

where $a$ and $b$ are constants. This equation leads to an equation for the coverage of the surface itself being given by eqn. (2):

$$q = (1/b)\ln(t) + k \quad (2)$$

where $k$ is also a constant. Thus, the probability of adsorption of an $NO_2$ gas molecule decreases exponentially as a function of the number of $NO_2$ molecules already adsorbed. Fig. 8 shows the plot of the decrease in the Soret band intensity (this is proportional to the coverage) *versus* $\ln(t)$. The relationship is linear until high values of $t$ indicating that the Elovich model fits the surface adsorption process well. The deviation from linearity at high $t$ results from the slow diffusion process in which $NO_2$ diffuses into the buried layers of the film.

Of specific use here, however, are the parameters, $t_{50}$ ($t_{90}$) (the time taken for the Soret band intensity to fall to 50% (90%) of its final saturated value) used to characterise the speed of response and recovery. Table 1 indicates these values for both the response phase and the recovery phase. The $t_{50}$ for the response phase at 293 K is relatively fast compared to many other reports of organic gas-sensing materials at room temperature[12] and is of some interest commercially. Typically, many phthalocyanines have yielded $t_{50}$ response times around 5–10 minutes. The improved response time of EHO assemblies prepared by ultra-fast deposition is attributed to their enhanced surface area compared to conventional LB films.

The response of gas sensors as a function of gas concentration is important as it indicates the range of concentration over which the response is linear and yields the sensitivity. Fig. 9 represents a sequence of gas exposure–recovery cycles performed for different concentrations of $NO_2$ gas over the range 0.88–4.4 ppm. For all concentrations, the temperature of the sample was 293 K for the exposure phases and 353 K for each recovery phase. Heating and cooling between these temperatures using the Peltier device took only ~20 s. The figure clearly shows that the response increases with increasing concentration. Fig. 10 (inset) shows the magnitude of the optical response (total change in Soret band absorbance during

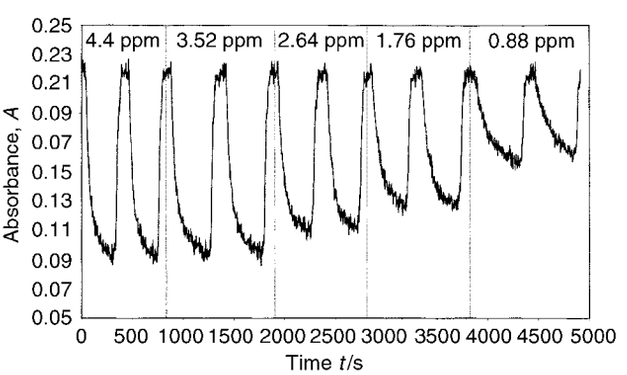


**Fig. 9** A sequence of gas exposure ($NO_2$)–recovery ($N_2$) cycles performed over the concentration range 0.88–4.4 ppm.

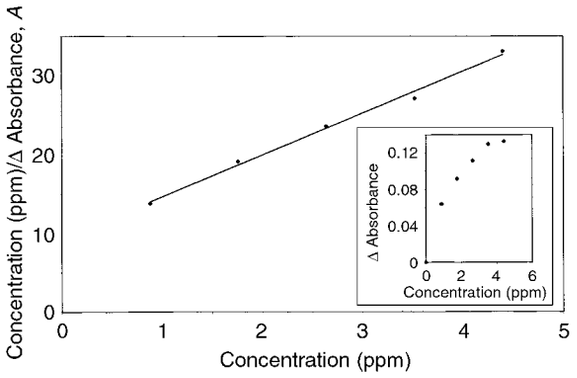


**Fig. 10** Langmuir adsorption plot for an EHO LB film. (Inset: Change in Soret band absorbance (for saturation) as a function of $NO_2$ gas concentration.)

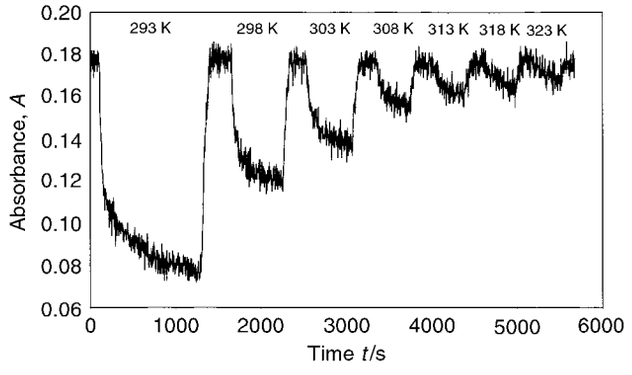


**Fig. 11** A sequence of exposure cycles performed over the temperature range 293–323 K. The temperature for the recovery phase is 353 K in all cases.

a gas exposure cycle) as a function of the gas concentration. This curve is commonly observed in cases in which Langmuir adsorption occurs. Langmuir's adsorption theory[13] suggests that a plot of $c/\Delta$Abs *versus* $c$ (where $\Delta$Abs is the change in Soret band absorbance and $c$ is the gas concentration) should yield a straight line if the assumptions on which it is based are valid. These assumptions are that the activation energy for adsorption is the same for all binding sites in the thin film assembly, that there is no motion of adsorbed $NO_2$ molecules over the surface and that $NO_2$ molecules striking a surface site that is already occupied do not adsorb. This latter assumption limits the adsorption of $NO_2$ onto a thin organic film surface to a single monolayer. Fig. 10 shows that a highly linear relationship is indeed obtained. Even though the Langmuir model ignores lateral interactions between adsorbed $NO_2$ molecules, surface mobility, surface heterogeneity and the possibility of adlayers‡ thicker than one monolayer, it nevertheless provides a basic understanding of the adsorption process for thin film assemblies of EHO and $NO_2$. Other more complex models such as the Braunauer–Emmett–Teller model[13] allow multilayer adsorption to occur and will be investigated in future studies in order to observe whether an improved theoretical understanding of the experimental data results.

The magnitude of the optical absorbance change of the Soret band, and the rate of response and recovery, are also temperature dependent parameters. Fig. 11 shows a sequence of exposure cycles performed over a range of temperatures. In all cases, the recovery phase is exacted at an elevated

‡An adlayer is the layer (or layers) of material deposited during one decomposition cycle.

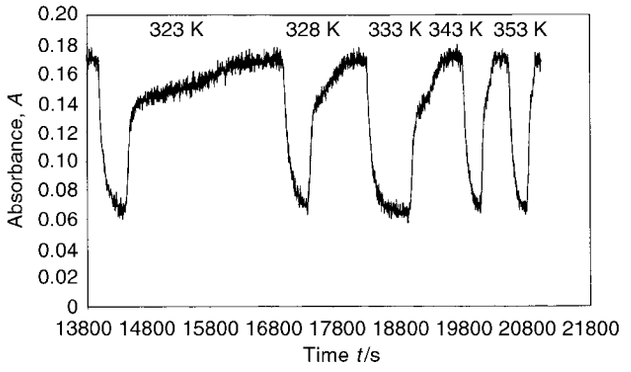


**Fig. 12** Temperature dependence of the recovery phase over the range 323–353 K. The temperature for the exposure phase is 293 K in all cases.

temperature of 353 K. It can be seen that the optical response to the gas exposure decreases rapidly as the sample temperature increases. This is expected since the dynamic equilibrium position between adsorption and desorption of $NO_2$ is shifted towards desorption as the temperature rises.

Fig. 12 shows the Soret band absorbance as a function of time for a sequence of exposure–recovery cycles in which the temperature during the gas exposure was maintained at 293 K, but the temperature of the recovery phase was varied over the range 323–353 K. It can be clearly seen that the rate of recovery is accelerated as the sample temperature increases; again, this arises as a result of the shift in the dynamic equilibrium position in favour of desorption. The specific form of the recovery process shows several distinct stages that probably represent desorption from surface or bulk sites possessing different $NO_2$ binding strengths. Such variation in binding strength may arise due to surface heterogeneity. This result, combined with the temperature dependence of the optical response during $NO_2$ exposure, indicates that the optimum operating conditions for sensors based on EHO are to cycle between 293 K and 353 K for the exposure and recovery cycles respectively. In this way, fast response and recovery rates can be achieved.

## Summary and conclusions

The optical absorbance spectrum of thin film assemblies containing EHO has been shown to be highly sensitive to low concentrations of $NO_2$. Thin film assemblies prepared using an ultra-fast LB deposition method have yielded a $t_{50}$ response time of $\sim$20 s. Relative absorbance changes of around 60% for 4.4 ppm $NO_2$ have been found. The morphology of these assemblies has been studied using atomic force microscopy; the deposited films contain isolated domains which themselves contains grains of around 30 nm diameter. Future work will focus on studying the sensitivity of EHO assemblies to other toxic gases such as $Cl_2$ and HCl, in order to examine its selectivity. Further kinetics modelling over a range of temperature will also be performed to further develop our understanding of the adsorption and desorption processes active in this sensing system. In this way, activation energies for the adsorption and desorption processes will be obtained.

## Acknowledgement

The authors would like to thank former members of the group for their initial involvement in this gas sensing project, particularly Dr Chris George and Dr Ginny Smith. We would also like to thank TQ Environmental plc for their interest in this work and EPSRC for the provision of a PhD studentship.

## References


1 W. Gopel, J. Hesse and J. N. Zemel, *Sensors: A Comprehensive Survey. Volume 2. Chemical and Biochemical Sensors*, 1991, VCH, Weinheim, Part 1, p. 34.
2 R. Das and P. D. Blanc, *Toxicol. Industrial Health*, 1993, **9**, 439.
3 P. T. Moseley, J. O. W. Norris and D. E. Williams, *Techniques and mechanisms in gas sensing*, Adam Hilger, Bristol, 1991.
4 M. C. Lonergan, E. J. Severin, B. J. Doleman, S. A. Beaber, R. H. Grubb and N. S. Lewis, *Chem. Mater.*, 1996, **8**(9), 2298.
5 S. Capone, S. Mongelli, R. Rella, P. Siciliano and L. Valli, *Langmuir*, 1999, **15**(5), 1748.
6 L. R. Milgrom, *The Colours of Life*, Oxford University Press, Oxford, 1997.
7 T. Richardson, V. C. Smith, R. A. W. Johnstone, A. J. F. N. Sobral and A. M. d'A, Rocha-Gonsalves *Thin Solid Films* 1998, **327–329**, 3151.
8 C. D. George, T. Richardson, M. E. Hofton, C. M. Vale, M. G. M. Neves and J. A. S. Cavaleiro, *Mater. Sci. Eng. C*, 1999, **8–9**, 559.
9 I. R. Peterson, G. J. Russell and G. G. Roberts, *Thin Solid Films*, 1983, **109**(4), 371.
10 The following paper O. Worsfold, C. M. Dooling, T. H. Richardson, M. O. Vysotsky, R. Tregonning, C. A. Hunter and C. Malins, *J. Mater. Chem.*, in the press, DOI:10.1039/b006344o.
11 M. C. Manchado, J. M. Guil and A. R. Paniego, *J. Chem. Soc., Faraday Trans.*, 1989, **85**(7), 1775.
12 A. K. Ray, M. J. Cook, S. C. Thorpe and S. Mukhopadyay, *Phys. Status Solidi A*, 1993, **140**(2), K85.
13 J. B. Hudson, *Surface Science: An Introduction*, Wiley, Chichester, 1998.